Influence of the Porous Structure of the Cathode on the Discharge Capacity of Lithium-Air batteries

Kazuki Sakai, Shinichiroh Iwamura*, Shin R. Mukai*

Graduate School of Engineering, Hokkaido University

N13W8, Kita-ku, Sapporo 060-6828, Japan

*Corresponding author. N13W8, Kita-ku, Sapporo 060-6828, Japan

E-mail address:iwamura@eng.hokudai.ac.jp (S.Iwamura)

E-mail address:smukai@eng.hokudai.ac.jp (S. R. Mukai)

Fax: +81-11-706-6593

Abstract

In the development of lithium-air batteries, to understand how the porous structure of the cathode affects the performance of the battery system is important because the main electrochemical reaction which occurs in this system is the deposition of Li_2O_2 in the pores of the cathode. To clarify the relationship between the porous structure of the cathode and the performance of the battery system, we used carbon gels with different pore size distributions as model cathodes and investigated how their pores are filled during discharging by analyzing the structure of cathodes discharged to different depths through N_2 adsorption experiments. The dominant deposit formed during discharging was identified to be Li_2O_2 by X-ray diffraction. Interestingly, the ratio of the volume of the Li_2O_2 deposited in fully discharged cathodes to the meso-macropore volume of the cathode was in the range of 0.5-0.6 and was fairly constant among the samples. Such ratios are higher than those of microporous carbon cathodes such as activated carbon cathodes. These results suggest that increasing the meso-macro pore volume of the cathode is effective to obtain large capacities in lithium-air batteries.

Introduction

Lithium-air batteries have drawn a lot of attention as they are expected to become a promising secondary battery system for electric automobiles due to its high theoretical energy density (11680 Wh/(kg-Li)), which is close to that of gasoline (13000 Wh/kg)[1]. This battery system uses oxygen and metal lithium for the cathode active material and the anode active material, respectively. For the electrolyte, organic electrolytes, ionic liquid electrolytes or polymer electrolytes can be used[2-5]. Presently, organic electrolytes such as tetra (ethylene) glycol dimethyl ether (TEGDME) are typically used [3] [6-9]. A remarkable advantage of the lithium-air battery system is that the cathode active material (i.e. O_2) can be taken into the battery cell from air so there is no need for it to be stored in the battery cell. Due to this advantage, the weight and volume of lithium-air batteries can be reduced, which leads to a high energy density.

Lithium-air batteries using organic electrolytes are operated through the reactions shown in (1), (2).

Cathode: $2Li^+ + O_2 + 2e^- \leftrightarrow Li_2O_2$ (1)

Anode: $Li \leftrightarrow Li^+ + e^-$ (2)

Solid Li_2O_2 deposits on the surface of the cathode during discharging and it decomposes to Li^+ and O_2 during charging. The cathode needs to have a large surface area and void

space to accommodate Li_2O_2. Thus, porous materials are selected for the cathode and needless to say their structure significantly affects the performance of the battery.

In the past few years, some researchers have studied how the porous structure of the cathode affects the performance of lithium-air batteries [10-12]. Although the surface area for Li_2O_2 deposition during discharging was expected to govern discharge capacities, the BET surface area of the cathode was found not to strongly affect discharge capacities in a previous report[10]. On the discharge at a high areal current density of 1 mA/cm^2 in a battery system using propylene carbonate as the electrolyte, discharge capacity linearly increases with the increase in average pore diameter rather than the increase in the total surface area of the cathode [12]. BET surface area strongly depends on the degree of development of micropores whose diameter is below 2 nm and these pores are thought to be too small for efficient Li_2O_2 deposition. Thus, pores wider than micropores are needed for efficient deposition. How mesopores affect capacity was investigated using mesocellular carbon foams and it was found that the capacity of lithium-air batteries can be significantly increased by adjusting the mesoporous structure of the carbon[11]. Mesopores are also thought to be useful to increase the accessibility of O_2 and Li^+ to the carbon surface[13]. Thus, proper controlling of the mesoporous structure in the cathode is thought to be the key factor for improvement of

the performance of lithium-air batteries and the appropriate mesoporous structure needs to be clarified. In addition to the porous structure of the original carbon materials, the porous structure after cathode preparation is also important because binders affect the porous structure and the performance of lithium-air batteries [14].

To investigate how the porous structure of the cathode affects the performance of lithium-air batteries, carbon materials with tunable porous structure are useful. One example of such carbons is a carbon gel, which has a network structure composed of carbon nanoparticles and also has mesopores with fairly uniform pore size in its structure[15, 16]. Carbon gels can be obtained through the carbonization of resorcinol-formaldehyde (RF) gels[15-17]. The size of the mesopores of carbon gels can be easily controlled by adjusting preparation conditions. Due to this unique feature, carbon gels can be used as a model material to clarify the appropriate porous structure for cathodes of lithium-air batteries.

Some researchers have already studied the influence of porous structures using carbon gels as the cathode of lithium-air batteries. For example, Mirzaeian *et al.* reported that discharge capacities can be determined from the surface area, pore size and pore volume of the cathode[13]. Especially, mesopores in carbons can be used for efficient deposition during discharge and therefore the mesopore volume significantly

affects discharge capacity [18, 19]. In addition, it has been reported that the efficiency of Li_2O_2 deposition within mesoporous carbon gels is higher than that of microporous activated carbons[19]. In these reports, pores in carbon gels were controlled only in the range of mesopores (2-50 nm) and influences of pores wider than mesopores were not surveyed even though the size of the pores of carbon gels can also be controlled in the range of small macropores. In addition, the structure of discharged carbon-gel cathodes was not characterized in detail and how the porous structure changes during discharging remains unclear.

In this study, we investigated how the porous structure of the cathode affects the capacity of lithium-air batteries by using carbon-gel cathodes which pore sizes were varied in a wide range. Deposits in the carbon-gel cathodes were identified by X-ray diffractometry and X-ray photoelectron microscopy, and the changes in porous structure during discharging were characterized by N_2 adsorption experiments. Based on the obtained results, we intend to propose an appropriate porous structure of carbon cathodes for lithium-air batteries.

Experimental

Materials

Resorcinol (R, 99.0%), formaldehyde (F, 36.0 wt% aqueous solution stabilized by 5-10 wt% methanol), sodium carbonate (C, 99.8%), 2-methyl-2-propanol (99.0%), 1-methyl-2-pyrrolidone (99.0%) and tetrahydrofuran (99.5%) were purchased from Wako Pure Chemical Industries. Tetraethylene glycol dimethyl ether (TEGDME, 99.0%) and lithium trifluoromethanesulfonate (CF_3SO_3Li, 99.995%) were purchased from Sigma-Aldrich Corporation. Polyvinylidene difluoride (PVDF, KF Polymer #1100), lithium foil and carbon paper (TGP-H-060) were respectively purchased from KUREHA Corporation, Honjo Metal Corporation and Toray Industries.

Synthesis of carbon gels

Carbon gels were synthesized according to the literature[20]. Typically, R, C and F were mixed into distilled water (W). R/F and R/W were set to 0.5 mol/mol and 0.5 g/mL respectively. R/C was varied between 50 and 1500 to control the porous structure of carbon gels. The mixture was kept at 303 K until it transformed to a gel and then kept at 333 K for three days. Then, the gel was immersed into 2-methyl-2-propanol at 323 K for three days to exchange the water in it to this alcohol. In this process, 2-methyl-2-propanol was refreshed twice a day. Then the gel was dried at 393K in air

for three days. The dried gel was carbonized in a quartz tube with an inner diameter of 20.8 mm at 1273 K under a 100 mL/min N_2 flow. In this process, the tube was heated to 523 K at a ramp rate of 3.75 K/min and kept at 523 K for two hours, then heated to 1273 K at a ramp rate of 4.17 K/min and kept at 1273 K for four hours. After cooling to room temperature, the carbon gel was collected. The obtained carbon gel was labeled by the R/C value it was synthesized at.

Fabrication of carbon cathodes

The resulting carbon gel was milled at 600 rpm for 10 minutes by a planetary ball mill (FRITSCH, premium line p-7) using balls and a vessel made of agate. The resulting powdery carbon gel was mixed with a 12% solution of PVDF in 1-methyl-2-pyrrolidone at a weight ratio of 19/1 (carbon gel / PVDF) for three minutes using a mixer (Thinky, AR-100). The mixture was coated on a carbon paper at a thickness of 50 μm. The coated carbon paper was dried at 388 K under vacuum for 15 hours and then circles with a diameter of 16 mm were punched out from it using a punching tool. The amount of the carbon gel loaded on the circles was in the range of 2.1-4.6 mg/cm^2.

Electrochemical measurements

Coin-type cells are suitable for practical battery tests, but it is difficult to recover the discharged cathodes without damaging them. Swagelok-type cells can be easily disassembled and the discharged cathodes can be recovered easily. Therefore, coin-type cells and Swagelok-type cells were respectively used to evaluate cathode performance and to obtain samples for the observation of the surface of discharged cathodes. Note that the performance of the cathodes in Swagelok-type cells is not very different from that in coin-type cells. These cells were assembled in a glove box filled with Ar. Water and oxygen concentrations in the glove box were kept under 1 ppm. Figure 1 shows the configuration of the cells. Coin-type cells have holes in their cathode cap so that oxygen can be supplied to the cells. In the Swagelok-type cell, O_2 was supplied through a stainless mesh. The separator was a glass filter (GF/A, Whatman) and the electrolyte was a solution of CF_3SO_3Li in TEGDME (TEGDME: CF_3SO_3Li = 4:1, molar ratio).

The cells were placed in an air-tight box (Figure 2) into which oxygen was supplied at 10 mL/min. They were discharged and charged in the range of 2.0-4.4 V at a current density of 50 mA/(g-carbon gel) after 10-hours rest in an oxygen atmosphere.

Discharged Swagelok-type cells were disassembled in a glove box filled with argon and the cathodes were taken out. After the cathodes were soaked in TEGDME for 12 hours to remove CF_3SO_3Li, they were washed with tetrahydrofuran to remove

TEGDME. Then, the cathodes were dried at room temperature in a glove box.

Characterization

The porous structure was characterized by nitrogen adsorption experiments conducted at 77 K using an adsorption apparatus (BELSORP mini or BELSORP max, Microtrac Bel). Prior to adsorption experiments, carbon-gel powders were dried at 523 K under a N_2 flow for four hours and carbon-gel cathodes were cut into strips and dried at 423 K under vacuum. Specific surface areas of the samples were calculated from Brunauer-Emmett-Teller (BET) plots and pore volumes were calculated from N_2 uptakes. Pore size distributions were calculated using the Dollimore-Heal (DH) method. Deposits in carbon-gel cathodes after discharging were identified by X-ray diffractometry (XRD, Ultima IV, Rigaku) and X-ray photoelectron spectroscopy (XPS, JPS-9200, JEOL). For XRD measurements, samples were fixed on a Si sample holder with a cover to prevent air exposure (see Figure S1 in the supporting information) and measured at 40 kV and 20 mA using CuKα radiation. In XPS measurements, samples were set on indium foils and measured using MgKα radiation. To minimize air exposure, the samples were put in a sealed box and transferred from the glove box and was set in the XPS apparatus just before measurements.

Results

Porous structures of carbon gels prior to and after cathode preparation were characterized by N_2 adsorption experiments. As-prepared powdery carbon gels originally have micropore volumes in the range of 0.25-0.33 cm^3/g (Table I), but these volumes decrease to 0.02-0.12 cm^3/g after cathode preparation. While it was reported that the binder affected the porous structure of the cathode [14], the decreases should be caused not only by the binder because the amount of the binder used in this study is only 5wt%, which can be converted to 0.03 (cm^3-binder)/(g-carbon) using the density of the binder (1.78 g/cm^3). This decrease in micropore volume may be because NMP, which is used as the solvent of the binder for preparing the cathodes, fills or clogs the inlets of the micropores in the carbon gels. Microporosity in carbon-gel cathodes can be recovered at 573 K (Figure S2) but this temperature is higher than the melting point (447 K) of the PVDF binder. As mentioned above, it has been reported that micropores in the cathodes hardly contribute to the capacity of lithium-air batteries because they are too small to incorporate Li_2O_2. Thus, although they affect microporosity, PVDF binder and NMP can be used to prepare cathodes for battery tests. Figure 3 shows N_2 adsorption isotherms and pore size distributions of cathodes prepared using carbon gels

synthesized under different R/C values. Mesopore volumes (V_{meso}) and meso-macro pore volumes ($V_{meso\text{-}macro}$), which means the summation of mesopore volumes and macropore volumes, in table I were calculated by subtracting N_2 uptakes at $P/P_0 = 0.20$ from those of $P/P_0 = 0.96$ and $P/P_0 = 0.99$, which correspond to pore diameters of 50 nm and 200 nm, respectively. In all samples, N_2 uptake significantly increased at $P/P_0 > 0.6$, which means that the samples have developed mesopores and/or macropores. From the pore size distributions derived from the isotherms, it can be confirmed that the pore sizes of mesopores or macropores increase with the increase in the R/C value, which is a well-known character of carbon gels[21]. Although the mesopore volumes and meso-macro pore volumes varied with the R/C value, they didn't significantly change after cathode preparation. Thus, it can be concluded that pore volumes of carbon-gel cathodes can also be controlled by varying the R/C value that the carbon gels are synthesized at.

Figure 4 shows discharge-charge curves of cathodes prepared using carbon gels synthesized at different R/C values. The voltage during discharging of the cathodes was approximately 2.7 V and the initial voltage during charging was about 3.8 V. This voltage gradually increased to 4.4 V with the progress of charging, which agrees with reported studies[13, 18, 19, 22]. The specific capacity first increases with the increase in the

R/C value of the carbon gel used for cathode preparation, and after R/C reaches 500, it starts to decrease. This trend suggests that the specific capacity is affected not only by the size of pores in the cathode but also by other factors such as the volume of such pores.

The deposits in a discharged cathode were identified by XRD and XPS. In the lithium-air battery system, the formation of various byproducts during discharging were reported [2, 23-28]. Because byproducts are generally generated through the decomposition of salts and solvents of the electrolyte, the electrolyte largely affects the species of the generated byproducts. In this study, CF_3SO_3Li and TEGDME were respectively used as the salt and the solvent. This electrolyte has been reported to have a high stability [3, 27, 28], but the generation of some byproducts from it, such as Li_2CO_3, LiOH, carboxylate and LiF have been reported [27, 29]. Among them, Li_2CO_3 and LiOH have been mainly reported as the byproducts in various electrolytes [23-28] although they can also reversibly charge and discharge in some cases [30, 31]. Figure 5 shows XRD patterns of a typical carbon-gel cathode (R/C1000) measured prior to and after discharging for 20 hours. The cathode contains carbon gel, carbon paper and PVDF. Peaks at 43.0° and 54.5° of the cathode prior to discharging are identified as the (10) and (004) reflections of carbon, respectively, originating from the carbon paper (Figure S3).

Crystalline Li_2O_2 clearly forms on the cathode during discharging. In previous reports, Li_2CO_3 and LiOH are deposited as crystalline byproducts, which can be confirmed by XRD measurements as peaks at 38.1° and 32.5°, respectively [23-25]. While XPS analysis suggests the presence of them (see the supporting information), corresponding peaks are not observed in the XRD pattern in Figure 5b. This indicates that the amount of the major byproducts is much smaller than that of Li_2O_2. Therefore, it can be regarded that the major byproduct, Li_2CO_3 and LiOH, and other crystalline byproducts hardly deposit in the cathodes during discharging and the dominant deposit in this system is Li_2O_2.

To investigate how pores are filled with deposits during discharging, cathodes discharged to different depths were prepared and their porous structure was characterized through N_2 adsorption experiments. Figure 6 shows N_2 isotherms and pore size distributions of R/C200, 500, 1000 cathodes discharged to different depths. In this investigation, carbon-gel cathodes were discharged for 10 hours or to a predetermined end voltage (2.0 V). Carbon gels were coated on the carbon paper at a thickness of 50 μm, which value is much smaller than the reported deposition depth [32]. Therefore, the deviation of the deposit distribution in the cathode does not need to be considered in this study. In the case of the R/C200 cathode, the N_2 uptake amount of the cathode after discharging for 10 hours in the range P/P_0=0.20-0.96 significantly

decreased, which means that mesopores are filled with deposits. The N_2 uptake amounts of the cathode after discharging to 2.0 V in the same P/P_0 range further decreased, suggesting pores are further filled with deposits. While the mesopore volume of the cathode decreased with the increase in the depth of discharging, the volume of pores with a radius in the range of 25-100 nm, which corresponds to the volume of voids naturally formed between carbon gel particles, also decreased. This suggests that such voids are also used for Li_2O_2 deposition. In the R/C500 and R/C1000 cathodes, while the N_2 uptake amounts of the cathodes after discharging for 10 hours in the range of P/P_0>0.90 decreased, those in the range of P/P_0<0.90 increased. In addition, the peak position of the pore size distributions shifted to the left when the depth of discharging was increased. These results indicate that larger pores are filled by Li_2O_2 and get narrower. After discharging to 2.0 V, all of the carbon-gel cathodes still have pores in a similar extent, suggesting that the pores in the cathode cannot be completely used for Li_2O_2 deposition. To investigate the appropriate porous structure for Li_2O_2 deposition, it is necessary to know how efficiently pores with different sizes can contribute to Li_2O_2 deposition. This will be discussed in the next section.

Discussions

Assuming that the deposit formed during discharging is only Li_2O_2 and that deposition

occurs uniformly on the inner surface of a carbon gel, the thickness of the deposit ($d_{Li_2O_2}$) in the cathodes was calculated from the discharge capacity, the density of Li_2O_2 and the BET surface area of the cathode (Table II). As shown in Table II, $d_{Li_2O_2}$ increases when the R/C value of the carbon gel in the cathode is increased from 200 to 500, and the $d_{Li_2O_2}$ of cathodes prepared using R/C500-1500 carbon gel are roughly the same. Viswanathan *et al.* reported that the calculated $d_{Li_2O_2}$ of a Li_2O_2 layer formed on a flat surface of a glassy carbon at a current density of 1 μA/cm^2 is 4-5 nm[33]. Because this value is close to that of the cathodes made using R/C500-1500 carbon gels, the surface of pores in these cathodes are thought to be sufficiently used for deposition during discharging. $d_{Li_2O_2}$ of R/C200 is smaller than those of R/C500-1500, suggesting that most of the micropores in R/C200 are too small to accommodate Li_2O_2 crystals or are too small for the reactants to efficiently diffuse into them to effectively utilize their whole volume. Thus, micropores are thought not to be effective pores for Li_2O_2 deposition.

Next, how the structure of mesopores and macropores of the cathode affects discharge capacity is investigated. Since the discharge capacity increases with the increase in the meso-macro pore volume of the cathode, the ratios of deposited Li_2O_2 volume to pore volume of the cathode samples are compared (Figure 7). As shown in Figure 7, the deposited Li_2O_2 volume to mesopore volume ratios ($V_{Li_2O_2}/V_{meso}$) vary, and

some of them are higher than 1. This means that deposition occurs not only in mesopores but also in macropores. On the other hand, the deposited Li_2O_2 volume to meso-macro ($V_{Li2O2}/V_{meso\text{-}macro}$) and total pore volume (V_{Li2O2}/V_{total}) ratios are roughly constant. The total pore volume means the summation of the volumes of micropores, mesopores and macropores, but the volumes of micropores which exist in the carbon-gel cathodes are extremely small as mentioned above. Thereby, the total pore volumes are almost the same as the meso-macro pore volumes. The almost constant and fairly high $V_{Li2O2}/V_{meso\text{-}macro}$ values indicate that the meso-macro pore volume of the cathode significantly affects the discharge capacity. Thus, in order to show a large discharge capacity the cathodes of lithium-air batteries need a large volume of meso-macro pores. Table III shows the V_{Li2O2}/V_{total} values of carbon materials studied in previous reports. In Table III, the V_{Li2O2}/V_{total} values of carbon blacks, carbon nanotubes and graphene nanosheets are higher than 1, which may be because in these materials their outer surface is mainly used for Li_2O_2 deposition and due to the flexibility of the structure of their aggregates the volumes of the voids formed in their aggregations cannot be accurately evaluated by N_2 adsorption experiments. Thus, these materials cannot be compared with carbons with a rigid structure, like carbon gels. In Table III, the V_{Li2O2}/V_{total} values of carbon gels are mostly around 0.3 and the V_{Li2O2}/V_{total} values of

activated carbons are in the range 0.01-0.18, suggesting that the pores of carbon gels can be effectively used for Li_2O_2 deposition when compared with those of activated carbons. This is because carbon gels are generally mesoporous and/or macroporous, and their porous structures can be adequately controlled. The carbon gels prepared in this work show high $V_{Li2O2}/V_{meso\text{-}macro}$ values close to 0.6, regardless of pore size, because they are mesoporous and/or macroporous rather than microporous. In conclusion, from the viewpoint of specific capacity, porous carbons having a large meso-macro pore volume are more suitable than microporous carbons like activated carbons, even though the latter tends to have a higher BET surface area.

Conclusion

Carbon gels with various pore size distributions were prepared and how the structure of cathodes for lithium-air batteries affects discharge capacity was investigated using cathodes prepared from them. While most of the micropores in the cathode disappeared in the process of cathode preparation, the structure of mesopores hardly changed. The surface of meso-macro porous carbon-gel cathodes is sufficiently used for Li_2O_2 deposition like a flat surface of a glassy carbon. Discharge capacities significantly

depended on the meso-macro pore volumes of the cathodes. Therefore, the ratios of deposited Li_2O_2 to meso-macro pore volume of carbon gels prepared in this work are constant (around 0.5-0.6), and higher than those of microporous carbons. From these results, it can be concluded that Li_2O_2 mostly deposits within both mesopores and macropores and can hardly deposit in micropores. Since the meso-macro pore volume strongly affects the discharge capacity, porous carbons having large meso-macro pore volumes are suitable for cathodes to obtain lithium-air batteries with large capacities.

Acknowledgements

This work was partly supported by the ALCA-SPRING of JST. The authors thank Dr. Yoshimi Kubo, chief researcher of NIMS-GREEN, and his team for their teaching us how to prepare coin-type cells of lithium-air batteries.

References

1. G. Girishkumar, B. McCloskey, A. C. Luntz, S. Swanson and W. Wilcke, *J. Phys. chem. Lett.*, **1**, 2193 (2010).
2. D. Xu, Z. L. Wang, J. J. Xu, L. L. Zhang, L. M. Wang and X. B. Zhang, *Chem. Commun.*, **48**, 11674 (2012).
3. H. G. Jung, J. Hassoun, J. B. Park, Y. K. Sun and B. Scrosati, *Nat. Chem.*, **4**, 579 (2012).
4. T. Kuboki, T. Okuyama, T. Ohsaki and N. Takami, *J. Power Sources*, **146**, 766 (2005).
5. K. M. Abraham and Z. Jiang, *J. Electrochem. Soc.*, **143**, 1 (1996).
6. H. G. Jung, Y. S. Jeong, J. B. Park, Y. K. Sun, B. Scrosati and Y. J. Lee, *Acs Nano*, **7**, 3532 (2013).
7. G. Y. Zhao, Y. N. Niu, L. Zhang and K. N. Sun, *J. Power Sources*, **270**, 386 (2014).
8. F. L. Lu, Y. R. Wang, C. Jin, F. Li, R. Z. Yang and F. L. Chen, *Journal of Power Sources*, **293**, 726 (2015).
9. G. G. Kumar, M. Christy, H. Jang and K. S. Nahm, *J. Power Sources*, **288**, 451 (2015).
10. J. Read, *J. Electrochem. Soc.*, **149**, A1190 (2002).
11. X. H. Yang, P. He and Y. Y. Xia, *Electrochem. Commun.*, **11**, 1127 (2009).
12. C. Tran, X. Q. Yang and D. Y. Qu, *J. Power Sources*, **195**, 2057 (2010).
13. M. Mirzaeian and P. J. Hall, *Electrochimica Acta*, **54**, 7444 (2009).
14. S. R. Younesi, S. Urbonaite, F. Bjorefors and K. Edstrom, *J. Power Sources*, **196**, 9835 (2011).
15. S. A. Al-Muhtaseb and J. A. Ritter, *Adv. Mater.*, **15**, 101 (2003).
16. H. Tamon, H. Ishizaka, M. Mikami and M. Okazaki, *Carbon*, **35**, 791 (1997).
17. T. Yamamoto, T. Sugimoto, T. Suzuki, S. R. Mukai and H. Tamon, *Carbon*, **40**, 1345 (2002).
18. G. O. Shitta-Bey, M. Mirzaeian and P. J. Halla, *J. Electrochem. Soc.*, **159**, A315 (2012).
19. S. B. Ma, D. J. Lee, V. Roev, D. Im and S. G. Doo, *J. Power Sources*, **244**, 494 (2013).
20. T. Tsuchiya, T. Mori, S. Iwamura, I. Ogino and S. R. Mukai, *Carbon*, **76**, 240 (2014).
21. H. Tamon, H. Ishizaka, T. Araki and M. Okazaki, *Carbon*, **36**, 1257 (1998).
22. F. Wang, Y. H. Xu, Z. K. Luo, Y. Pang, Q. X. Wu, C. S. Liang, J. Chen, D. Liu and X. H. Zhang, *J. Power Sources*, **272**, 1061 (2014).
23. Y. L. Li, J. J. Wang, X. F. Li, D. S. Geng, R. Y. Li and X. L. Sun, *Chem. Commun.*, **47**,

9438 (2011).

24. B. Sun, B. Wang, D. W. Su, L. D. Xiao, H. Ahn and G. X. Wang, *Carbon*, **50**, 727 (2012).

25. T. Zhang and H. S. Zhou, *Nat. Commun.*, **4** (2013).

26. S. A. Freunberger, Y. H. Chen, Z. Q. Peng, J. M. Griffin, L. J. Hardwick, F. Barde, P. Novak and P. G. Bruce, *J. Am. Chem. Soc.*, **133**, 8040 (2011).

27. E. Nasybulin, W. Xu, M. H. Engelhard, Z. M. Nie, S. D. Burton, L. Cosimbescu, M. E. Gross and J. G. Zhang, *J. Phys. Chem. C*, **117**, 2635 (2013).

28. M. Christy, A. Arul, A. Zahoor, K. U. Moon, M. Y. Oh, A. M. Stephan and K. S. Nahm, *J. Power Sources*, **342**, 825 (2017).

29. I. C. Jang, S. Ida and T. Ishihara, *Chemelectrochem*, **2**, 1380 (2015).

30. T. Liu, M. Leskes, W. J. Yu, A. J. Moore, L. N. Zhou, P. M. Bayley, G. Kim and C. P. Grey, *Science*, **350**, 530 (2015).

31. L. Qie, Y. Lin, J. W. Connell, J. T. Xu and L. M. Dai, *Angew. Chem. Int. Ed.*, **56**, 6970 (2017).

32. J. Nanda, H. Bilheux, S. Voisin, G. M. Veith, R. Archibald, L. Walker, S. Allu, N. J. Dudney and S. Pannala, *J. Phys. Chem. C*, **116**, 8401 (2012).

33. V. Viswanathan, K. S. Thygesen, J. S. Hummelshoj, J. K. Norskov, G. Girishkumar, B. D. McCloskey and A. C. Luntz, *J. Chem. Phys.*, **135** (2011).

34. J. Yin, J. M. Carlin, J. Kim, Z. Li, J. H. Park, B. Patel, S. Chakrapani, S. Lee and Y. L. Joo, *Adv. Energy Mater.*, **5**, 8 (2015).

35. B. Sun, X. D. Huang, S. Q. Chen, P. Munroe and G. X. Wang, *Nano Lett.*, **14**, 3145 (2014).

Table captions

Table I. Textural properties of carbon-gel powder and carbon-gel cathodes.

Table II. Specific properties of carbon-gel cathodes.

Table III. Pore volumes and capacities of lithium-air batteries of various carbon materials.

Table I. Textural properties of carbon-gel powder and carbon-gel cathodes.

		S_{BET}[a]	V_{total}[b]	V_{micro}[c]	V_{meso}[d]	$V_{meso\text{-}macro}$[e]
R/C	State	m^2/g	cm^3/g	cm^3/g	cm^3/g	cm^3/g
200	powder	771	0.87	0.33	0.53	0.54
500	powder	701	1.14	0.30	0.72	0.85
1000	powder	646	1.23	0.26	0.42	0.97
1500	powder	625	0.86	0.25	0.24	0.61
200	cathode	292	0.88	0.12	0.59	0.76
500	cathode	157	1.08	0.07	0.80	1.01
1000	cathode	102	0.98	0.04	0.41	0.95
1500	cathode	55	0.59	0.02	0.19	0.56

a BET surface area S_{BET} was determined from the data at $P/P_0 = 0.05\text{-}0.10$

b Total pore volume V_{total} was calculated from the N_2 uptakes at $P/P_0 = 0.99$

c Micropore volume V_{micro} was calculated from the N_2 uptakes at $P/P_0 = 0.20$

d Mesopore volume V_{meso} was calculated from the N_2 uptakes at $P/P_0 = 0.96$ and V_{micro}

e $V_{meso\text{-}macro} = V_{total} - V_{micro}$

Table II. Specific properties of carbon-gel cathodes.

	S_{BET}	Q	d_{Li2O2}
R/C	m^2/g	mAh/g	nm
200	292	1088	1.4
500	157	1683	4.0
1000	102	1540	5.6
1500	55	821	5.6

Table III. Pore volumes and capacities of lithium-air batteries of various carbon materials.

Sample name	V_{total} cm^3/g	V_{meso} cm^3/g	i	Capacity mAh/g	V_{Li2O2} cm^3/g	V_{Li2O2}/V_{total} -	V_{Li2O2}/V_{meso} -	Material	Reference
ACPF800-15	1.04	0.84	70 mA/g	910	0.34	0.33	0.40	PF carbon gel	18
ACPF800-30	1.25	0.98	70 mA/g	1247	0.46	0.37	0.47	PF carbon gel	18
ACPF800-60	1.60	1.30	70 mA/g	1299	0.48	0.30	0.37	PF carbon gel	18
ACPF800-90	1.85	1.54	70 mA/g	1461	0.54	0.29	0.35	PF carbon gel	18
ACPF800-120	2.01	1.87	70 mA/g	1852	0.69	0.34	0.37	PF carbon gel	18
ACRF002–1123K	1.32	0.87	20 mA/g	630	0.23	0.17	0.26	RF carbon gel	13
ACRF002–1223K	1.12	0.75	20 mA/g	180	0.07	0.06	0.09	RF carbon gel	13

ACRF002–1273K	1.43	1.01	20 mA/g	740	0.28	0.20	0.28	RF carbon gel	13
ACRF003–1073K	1.2	0.95	20 mA/g	528	0.2	0.17	0.21	RF carbon gel	13
ACRF003–1123K	1.34	1.02	20 mA/g	880	0.33	0.25	0.32	RF carbon gel	13
ACRF003–1323K	2.20	1.73	20 mA/g	1290	0.48	0.22	0.28	RF carbon gel	13
YP-50F	0.55		20 mA/g	264	0.1	0.18		Activated carbon	19
CEP21S	0.85		20 mA/g	124	0.05	0.06		Activated carbon	19
Carbon aerogel	2.53		20 mA/g	4155	1.55	0.61		Carbon aerogel	19
CRF1500-40	1.02	0.85		13500	5.02	4.92	5.91	RF carbon gel	22
Carbon A	2.01	2.01	0.1 mA/cm^2	2220	0.83	0.41	0.41	conductive carbon	4
Carbon B	1.92	1.34	0.1 mA/cm^2	360	0.13	0.07	0.10	conductive carbon	4
Carbon C	0.82	0.22	0.1 mA/cm^2	22	0.01	0.01	0.05	Activated carbon	4

Carbon D	0.46	0.102	0.1 mA/cm^2	17	0.01	0.02	0.10	Activated carbon	4
GNSs		1.17	75 mA/g	8706	3.24		2.77	Graphene nanosheet	23
BP-2000		1.11	75 mA/g	1909	0.71		0.64	Carbon black	23
Vulcan XC-72		0.27	75 mA/g	1054	0.39		1.44	Carbon black	23
super C	0.22		210 mA/g	2600	0.97	4.41		Carbon black	34
CNTs	1.33		210 mA/g	5000	1.86	1.40		Carbon nanotube	34
GNRs	1.46		210 mA/g	5000	1.86	1.27		Graphene nanosheet	34
PGE1	1.9		200 mA/g	20310	7.56	3.98		Graphene nanosheet	35
PGE2	1.5		200 mA/g	29375	10.9	7.27		Graphene nanosheet	35
PGE3	1.15		200 mA/g	22458	8.36	7.27		Graphene nanosheet	35

Figure captions

Figure 1. Configuration of the coin-type cell (left) and the Swagelok-type cell (right).

Figure 2. Cells and air-tight boxes with channels for O_2 supply and conductive paths.

Figure 3. N_2 adsorption isotherms (a) and pore size distributions (b) of cathodes prepared using carbon gels synthesized using different R/C values.

Figure 4. Discharge-charge curves of cathodes prepared using carbon gels synthesized at different R/C values at 50 mA/g in 1 atm of O_2. The curves shown are those of the cycle in which the cathodes showed the largest discharge capacity.

Figure 5. X-ray diffraction patterns of a typical carbon-gel cathode (R/C1000) measured (a) prior to and (b) after discharging for 20 hours.

Figure 6. N_2 uptakes and pore size distributions of cathodes prepared using carbon gels

synthesized using different R/C values (a and b R/C200, c and d R/C500, e and f R/C1000). Curves labeled 1 are of samples prior to discharging. Curves labeled 2 are of samples after discharging for 10 hours. Curves labeled 2 are of samples after discharging to the predetermined end voltage (2.0 V).

Figure 7. $V_{Li2O2}/V_{mesopore}$, $V_{Li2O2}/V_{meso\text{-}macro}$, V_{Li2O2}/V_{total} values of cathodes prepared using carbon gels synthesized using different R/C values.

Figure 1

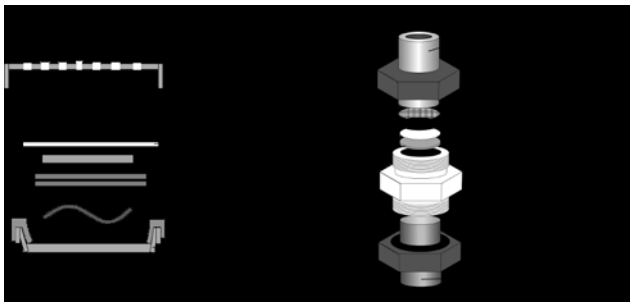

Figure 2

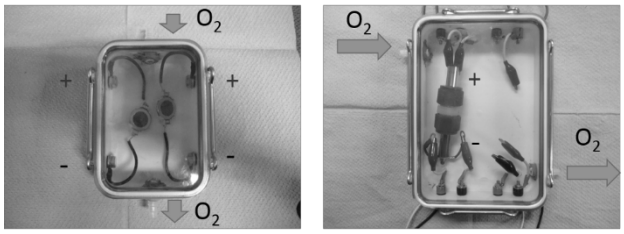

Figure 3

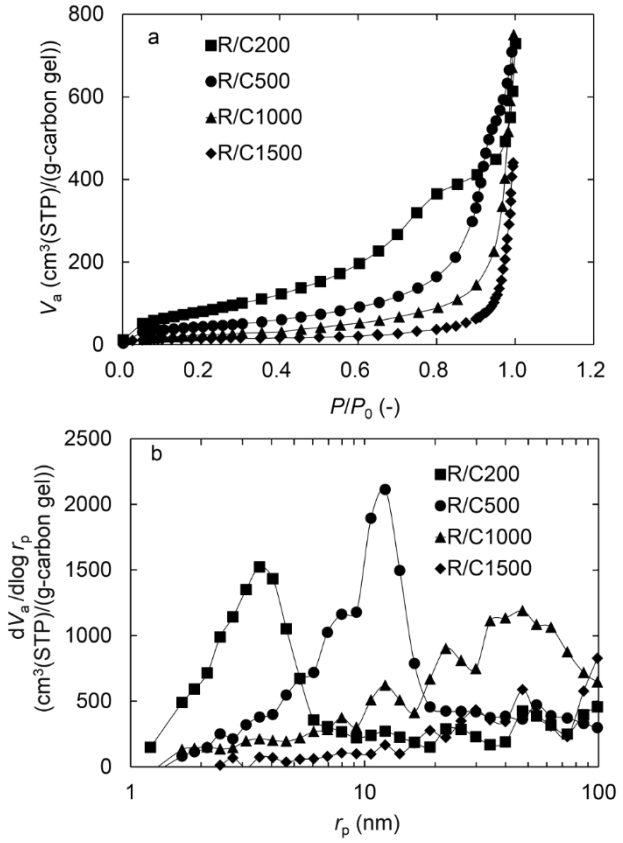
a
R/C200
R/C500
R/C1000
R/C1500
V_a (cm^3(STP)/(g-carbon gel))
P/P_0 (-)
b
R/C200
R/C500
R/C1000
R/C1500
$dV_a/d\log r_p$ (cm^3(STP)/(g-carbon gel))
r_p (nm)

Figure 4

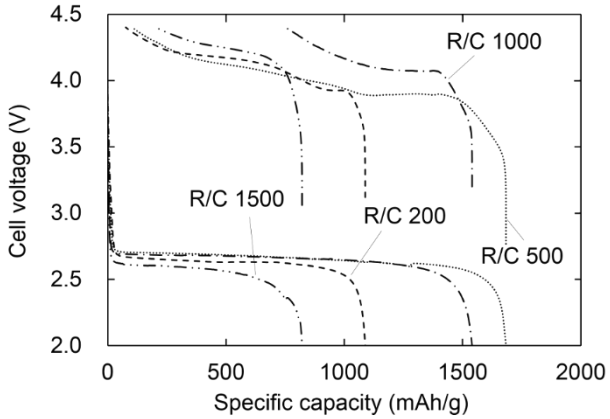
4.5
4.0
3.5
3.0
2.5
2.0
Cell voltage (V)
0
500
1000
1500
2000
Specific capacity (mAh/g)
R/C 1000
R/C 1500
R/C 200
R/C 500

Figure 5

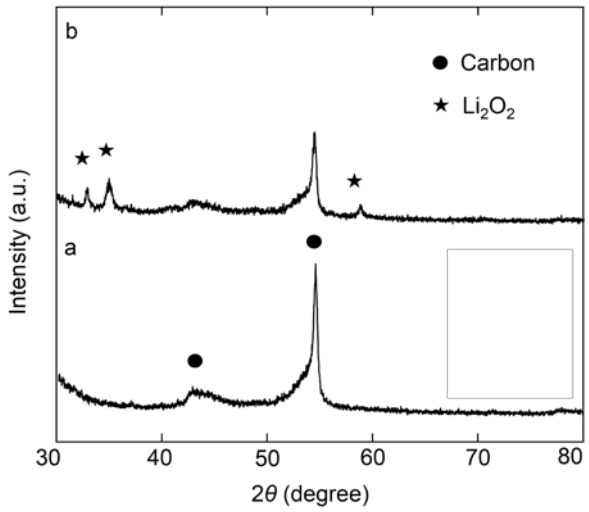

Figure 6

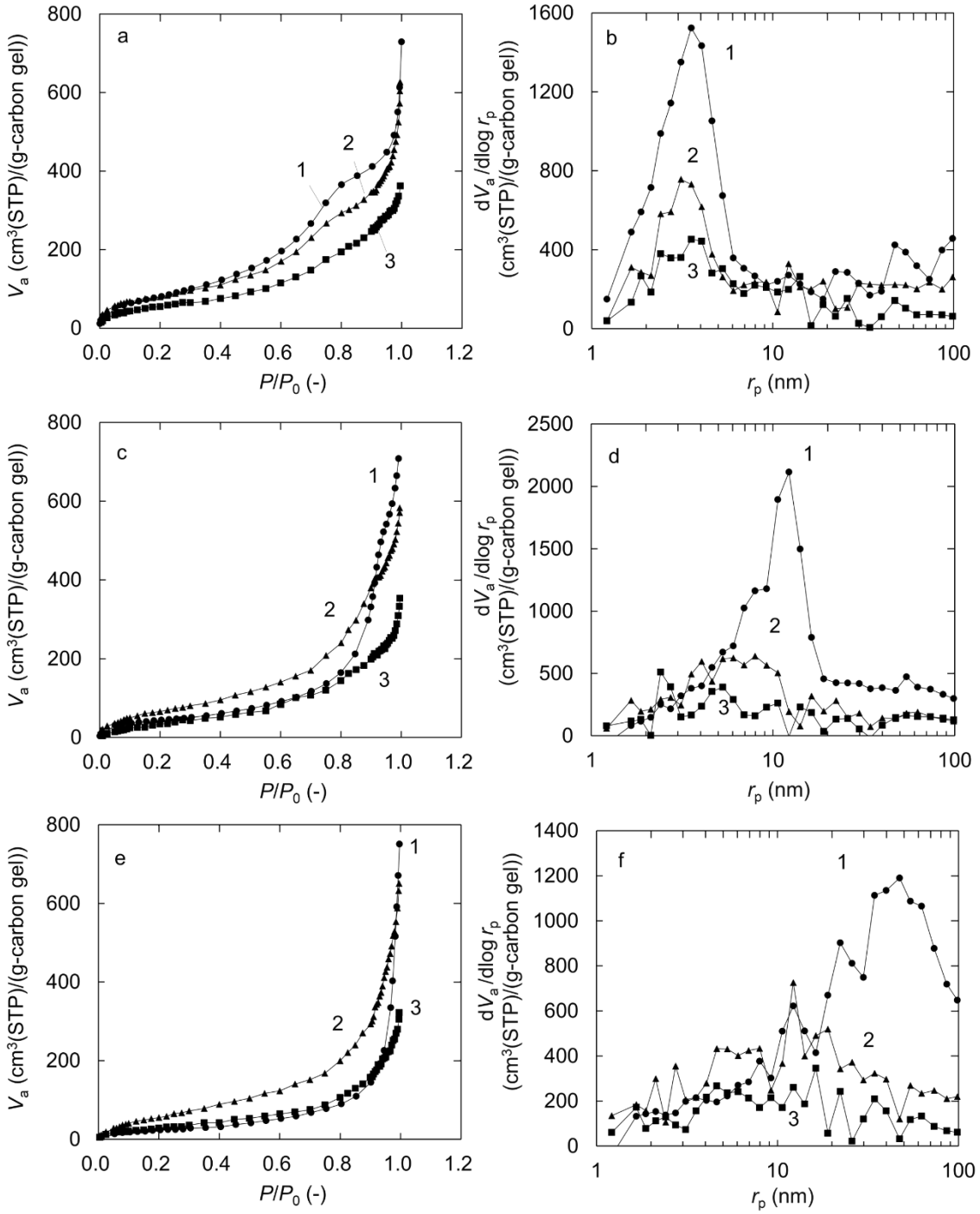
a
b
c
d
e
f
1
2
3
V_a (cm^3(STP)/(g-carbon gel))
P/P_0 (-)
dV_a/dlog r_p (cm^3(STP)/(g-carbon gel))
r_p (nm)

Figure 7

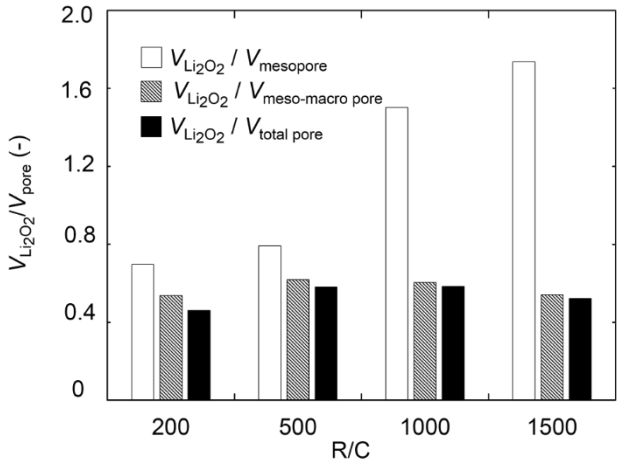
2.0
1.6
1.2
0.8
0.4
0
V_{Li2O2}/V_{pore} (-)
V_{Li2O2} / $V_{mesopore}$
V_{Li2O2} / $V_{meso\text{-}macro\ pore}$
V_{Li2O2} / $V_{total\ pore}$
200
500
1000
1500
R/C